Robust carbon-based electrodes for hydrogen evolution through site-selective covalent attachment of an artificial metalloenzyme

Regina E. Treviño, Jeffrey W. Slater,† Hannah S. Shafaat*

Department of Chemistry and Biochemistry, The Ohio State University, Columbus, OH. Shafaat.1@osu.edu

KEYWORDS Energy conversion, nickel, protein film electrochemistry, simulations, protein engineering, stability.

ABSTRACT: The use of biological systems for electrochemical energy conversion applications is often limited by instability of the protein or protein-electrode system. Here, we present a simple but efficient method for covalent attachment of nickel-substituted rubredoxin (NiRd), a model hydrogenase, to an unmodified graphite electrode based on amide bond formation. The resultant electrodes are shown to be highly active for H_2 evolution over a period of several weeks. The effects of different attachment methods on interfacial electron transfer (ET) rates and catalysis are investigated, with decreased ET rates and increased background reactivity observed for surface-modified electrodes. Electrochemical simulations reveal that reduced protein dynamics of the attached NiRd enzyme are likely responsible for decreased catalytic rates by modulating the intramolecular proton transfer step. Ultimately, this straightforward approach can be broadly applied to diverse redox-active proteins and enzymes and will expand the utility of such systems by conferring increased stability over extended periods of time.

INTRODUCTION The utilization of renewable hydrogen has gained traction due to its regard as a clean fuel.[1] However, current and traditional approaches for the production of hydrogen gas have several drawbacks, including the use of precious metal catalysts and generation of CO_2 as a byproduct. The utilization of enzymes as bioelectrocatalysts for fuel generation offers an alternative approach with distinct advantages, including high chemical specificity and catalytic rates, use of earth-abundant transition metals, and well-defined active sites and mechanisms.[2–4] For example, enzymes known as hydrogenases (H_2ases) have been optimized for efficient turnover using either iron or iron and nickel[5–7] and catalyze both the production of hydrogen from protons as well as hydrogen oxidation at almost the thermodynamic potential of the reaction, with relative activity that is dependent on the inherent bias of the enzyme.[8–10]s Fundamental studies of these enzymes have provided inspiration for the generation of small molecule mimics that also perform catalytic H_2 evolution or oxidation.[11–13] Though construction of synthetic models of enzyme active sites may provide access to similar reactivity, it is no surprise that the secondary and tertiary environments around the active site and the protein fold play significant roles in modulating the high levels of activity achieved by the naturally occurring systems.[14,15] Following from this reasoning, the utilization of stable protein scaffolds within which to reconstruct the active site may be a more effective approach to mimic not only the structure but also the activity of the native enzyme.[16–18]

Rubredoxins (Rd) are small (4.5-5.2 kDa), robust electron transfer proteins with a tetrathiolate, mononuclear metal binding site. The protein fold is remarkably resistant to a wide range of pH values, temperatures, solvents, and oxygen, as well as straightforward to express and stable towards mutagenesis.[19] While the protein natively binds iron (FeRd), it has been previously demonstrated that the active site metal can be easily replaced with a variety of different transition metals, such as nickel, zinc, copper and cobalt, without compromising the stability or protein fold.[20–23] This facile metal exchange renders Rd a particularly attractive system for the engineering of an artificial hydrogenase; the protein coordination environment of nickel-substituted rubredoxin (NiRd) closely resembles the active site structure at the nickel center of the [NiFe] H_2ase.[20,24,25] Prior work by our group and others has shown that NiRd serves not only as a structural mimic, but also as a functional and mechanistic model enzyme for the [NiFe] H_2ase.[20,25–27] Initial characterization of NiRd demonstrated that the protein is catalytically active towards hydrogen production.[25] Detailed mechanistic studies on the NiRd metalloenzyme resolved intrinsic electrocatalytic properties of the active site, metrics that are masked by the iron-sulfur cluster electron relay in the native enzyme.[26] In this way, studies of model systems can also provide insight into the properties of naturally occurring enzymes. As an additional advantage of the model system, changes to the active site primary, secondary, and outer coordination spheres

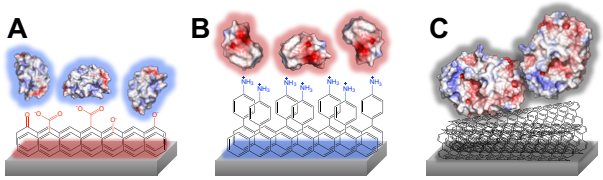

Figure 1. (**A**) The surface of unmodified graphitic electrodes is typically negatively charged, favoring electrostatic adsorption of positively charged proteins and molecules. (**B**) Aniline-functionalized surfaces are positively charged, favoring electrostatic adsorption of positively charged proteins and molecules. (**C**) Nanotube-coated surfaces are hydrophobic, favoring adsorption of large, hydrophobic, or zwitterionic proteins and molecules.

can be accomplished in a rational fashion as a means to improve or gain insight into the catalytic activity.[27,28]

Electrochemistry is a powerful and sensitive technique for the study of redox-active molecules. The study of electron transfer (ET) within proteins is of great relevance for understanding signaling pathways, metabolic processes, bioenergetics, and energy storage reactions within biological systems.[6,29] Both carbon-based and metallic electrodes have been used for the study of metalloproteins.[30,31] However, the observed signals rely heavily on the nature of the interaction between the protein and the electrode. Historically, the primary approach used to study redox enzymes has relied on simple adsorption of the protein to the electrode surface, forming predominantly monolayers of protein through a combination of electrostatic and hydrophobic interactions (**Figure 1**).[32] While this generally supports direct ET from the electrode surface to the biocatalyst,[33,34] eliminating the need for small-molecule mediators to serve as electron relays, orientation of the enzyme is not controlled and desorption can readily occur.[35]

To extend surface stability and control ET pathways, different approaches have been developed, ensuring the activity and intrinsic stability of the (bio)molecules are not compromised (**Scheme 1**).[36–40] One popular technique for the surface modification of electrodes harnesses the reactivity of the diazonium moiety.[36,41,42] This method relies on the reduction of a diazonium salt at the surface of a carbon-based electrode, forming a covalent carbon-carbon bond between the electrode and the resultant aryl radical accompanied by the release of nitrogen gas. A variety of diazonium salt derivatives are commercially available, allowing access to any desired functional group for further reactions.[41] In this study, 4-nitrobenzodiazonium is used because of the shelf stability of the reagent and facile electrochemical reduction of the nitroarene to an aniline. This functional group can act as an amine in carbodiimide cross-linking reactions to form amide bonds with carboxylic acids.[36] The aniline moiety can also participate in a three-component Mannich-type reaction along with formaldehyde for coupling to a phenol, as previously demonstrated for linking a fluorophore to a peptide.[43] While this is a facile method that offers access to a wide variety of surface-bound functional groups, the effectiveness is highly dependent on the conditions under which the diazonium modification takes place.[44] The aryl radicals can accumulate in multiple layers on the surface of the electrode, rather than a monolayer, resulting in an insulating layer forming between the electroactive surface and the sample in question and slowing ET significantly.

Carbon nanotubes (CNTs), are also used for surface modification.[45–47] CNTs are highly conductive, serve as effective electron mediators, provide high effective surface areas for the generation of large catalytic currents, and are amenable to functionalization, often through the use of pyrene derivatives.[45,48,49] Adsorption to the CNT occurs through π-π stacking interactions between the graphitic basal plane and the pyrene moiety, while specific chemical functional groups can be introduced off of the aromatic system.[47,50] However, this approach also has drawbacks. Layers of CNTs increase the capacitance of the electrode, making systems with small currents difficult to study. Biological molecules can adsorb to the surface as well as inside the nanotubes, giving rise to different orientations because of changes in hydrophobicity and polarity across the two sides of the tube.[51] Moreover, many of the commonly used methods for functionalization of CNTs result in highly reactive electrodes, which give rise to large background currents at negative potentials in aqueous environments.

The electrode surface itself can also be considered as a site for modification. A variety of graphitic carbon surfaces are used for the study of small molecules and biological systems, with differential reactivity that is attributed predominantly to the presence of defects.[50,52] The surface of aligned pyrolytic graphite (PG) subunits in a single sheet makes up the relativity inert "basal plane", while the ends of those stacked sheets make up the "edge plane", where most of the defects occur. These defective edges can react with air to form oxygen-containing functional groups, which can be utilized for surface tethering of molecules.[53] The edge plane also exhibits faster electron transfer than the basal plane.[48,50] However, even with these moieties, PG electrodes are largely unreactive towards proton reduction, rendering these surfaces attractive targets for direct functionalization.

In this work, multiple methods are developed and described for site-selective covalent attachment of Rd to the surface of carbon-based PG electrodes. We focus on modifications to the electrode surface that enable bioconjugation of the protein scaffold either via amide bond formation, using either a lysine, an

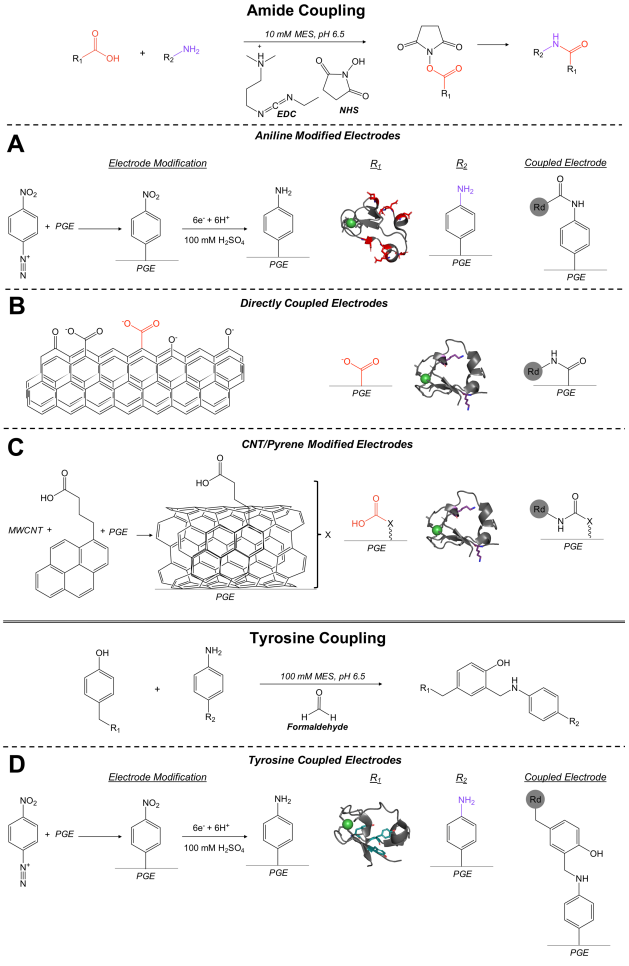

Scheme 1. Different methods for covalent attachment of Rd to a PG electrode surface relying on (***Top***) amide and (***Bottom***) tyrosine coupling strategies to (**A, D**) aniline-modified, (**B**) intrinsic carboxylic acid groups, or (**C**) CNT-pyrene surfaces.

aspartate, or a glutamate residue, or coupling through a tyrosine residue following a Mannich-type coupling (**Scheme 1**). Validation of the methodology and an investigation of the effects of controlled orientation on the rates of interfacial ET and overall catalytic activity of the wild-type (WT) NiRd enzyme and mutants are presented. Electrochemical simulations are used to investigate mechanistic changes upon attachment to the electrode surface, with reduced dynamics implicated in the lower absolute levels of activity observed. Importantly, the resulting optimized electrodes are stable over the timescale of many weeks and across a wide pH range, extending the potential applications of this artificial metalloenzyme towards environmentally benign, large-scale hydrogen evolution.

EXPERIMENTAL SECTION

Protein Expression, Purification, and Metal Substitution

Desulfovibrio desulfuricans ATCC 27774 wild-type rubredoxin and all mutants were heterologously expressed, purified, and metallated as previously described.[25–28] Protein purity was confirmed by native gel electrophoresis following metal substitution.

Fe^{II}Rd Preparation

Reduction of Fe^{III}Rd to Fe^{II}Rd in wild-type Rd and Rd mutants was carried out under nitrogen in an anaerobic glove box (O_2 < 2 ppm) (Vigor Technologies). A solution of Fe^{III}Rd was reduced by addition of 100 mM dithionite (DT) (Sigma-Aldrich), dissolved in 50 mM Tris buffer, pH 8.0, giving a distinct color change from dark red to clear. Excess reducing agent was removed by application of the protein solution to a self-packed PD-10 column equilibrated with 50 mM Tris, pH 8.0.[54] Protein fractions were collected and concentrated using a Centricon filtration concentrator (Millipore). A 2 µL aliquot of Fe^{II}Rd protein sample was oxidized by addition of 5 mM $K_3[Fe(CN)_6]$ under ambient conditions for concentration determination using optical spectroscopy. An extinction coefficient of 7,800 $M^{-1}cm^{-1}$ at 492 nm for Fe^{III}Rd was used.[26]

Surface Coupling Reactions

Covalent coupling of rubredoxin to the surface of pyrolytic graphite electrodes was carried out through carbodiimide crosslinker chemistry for the formation of a peptide bond between a carboxylate group and a primary amine supplied by either the electrode surface, an installed modification of the electrode surface, or the protein. Stock solutions of 1.5 M N-hydroxysuccinimide (NHS) (Sigma-Aldrich) and 1.8 M 1-ethyl-3-(3-dimethylaminopropyl) carbodiimide hydrochloride (EDC) (G-Biosciences) were freshly prepared in 10 mM MES (Fisher Scientific) buffer, pH 6.5. Appropriate volumes were added to glass culture tubes to achieve a final solution volume of 80 µL containing 200 µM total Rd, 72 mM NHS and 144 mM EDC. Freshly polished, home-made PG electrodes were submerged in solution and allowed to react for 1.5 hours. All electrodes were rinsed extensively with 50 mM Tris buffer, pH 8.0, to remove any adventitiously adsorbed Rd prior to electrochemical experiments and stored in 50 mM Tris buffer, pH 8.0, for stability experiments. Electrodes were prepared in triplicate to account for variability in protein coupling efficiencies across different electrodes.

Aniline Surface Modification

Aniline surface modification of PG was carried out through an aryl radical C-C coupling to the surface of the electrode followed by electrochemical reduction. A 100 mM solution of 4-nitrobenzenediazonium tetrafluoroborate ($[N_2Ar\text{-}NO_2][BF_4]$) (Sigma-Aldrich) in acetonitrile (Fisher Scientific) was freshly prepared, and 1 mL aliquots were dispersed in 20 mL scintillation vials. Freshly polished home-made PG electrodes were submerged and allowed to react for 5 minutes. Electrodes were then rinsed with acetonitrile to remove all excess reagents, quenched with ethanol, and subjected to a final rinse with deionized (MilliQ) water. Electrochemical reduction of the nitro group to the aniline derivative was carried out in an anaerobic glove box (O_2 < 2 ppm) by sweeping the potential from 0.6 to -0.9 V vs Ag/AgCl with a scan rate of 0.1 V/sec in an aqueous solution containing 100 mM H_2SO_4 according to Equation 1:

$$Ar - NO_2 + 6H^+ + 6e^- \rightarrow Ar - NH_2 \quad (1)$$

All electrodes were rinsed extensively with MilliQ water following electrochemical reduction to remove any excess acid. Covalent attachment of the protein to the aniline-modified electrodes was carried out using the carbodiimide crosslinking method described above or the Mannich-type coupling described below.

Carbon Nanotube and Pyrene Modification

Carbon nanotube (CNT)/pyrene-modified PG electrodes were achieved through a two-step process involving the deposition of a CNT layer followed by addition of a functionalized pyrene. First, a suspension of multiwalled (MW) CNTs (CheapTubes.com) in N'N-dimethyl formamide (DMF) (VWR) was formed by sonication of a 1 mg/mL solution for 15 minutes to achieve a uniform suspension. A 10 µL drop of the suspension was cast on the surface of home-made PG electrodes and allowed to fully dry overnight. A 1 mM solution of 1-pyrenebutyric acid (Acros Organics) in acetonitrile was freshly prepared, and 100 µL aliquots were transferred to glass culture tubes. The MWCNT-modified electrodes were submerged in the pyrene solution and allowed to sit for 1.5 hours. All electrodes were rinsed with MilliQ water to remove any excess pyrene from the surface and dried under vacuum. As with the aniline-modified electrodes, covalent attachment of the protein to the functionalized pyrene was performed using the methodology outline above for the carbodiimide crosslinking process.

Tyrosine Attachment via Mannich-Type Coupling

The methodology for coupling of Rd to the PG electrode surface via tyrosine residues was adapted from a prior report describing attachment of a fluorophore to tyrosine-containing peptides.[43,55] Home-made electrodes were modified using the aniline surface modification procedure outlined above. A solution was prepared with a final concentration of 25 mM formaldehyde (VWR) and 250 µM total Rd in 100 mM MES buffer, pH 6.5, and modified electrodes were submerged in solution. Electrodes were allowed to react overnight (~ 18 hours) at 4˚C. All electrodes were rinsed with 50 mM Tris buffer, pH 8.0, prior to electrochemical measurements.

Electrochemistry

All electrochemical experiments were conducted in a nitrogen glove box (O_2 < 2 ppm; Vigor Technologies) using a WaveNow potentiostat (Pine Research Instrumentation) or a CH Instruments 760E bipotentiostat for fast scan rate experiments. Experiments were performed in 150 mM sodium acetate buffer, pH 4.5. A multicomponent "CHAMP" buffer consisting of 25 mM CHES, 25 mM HEPES, 25 mM acetate, 25 mM MOPS and 50 mM potassium perchlorate (Sigma-Aldrich) was

utilized for pH dependence studies. All scan rate dependence experiments were conducted in 150 mM acetate buffer, pH 4.5, with saturating levels of potassium chloride. The pH of all buffers was adjusted using 1 or 10 M solutions of hydrochloric acid or potassium hydroxide. A three-electrode system was used for all experiments consisting of a homemade pyrolytic graphite (PG) working electrode (edge-plane) with a surface area of 0.09 cm^2, a platinum wire counter electrode (Alfa-Aesar) and an Ag/AgCl reference electrode (Pine Research Instrumentation). Homemade PG electrodes were constructed using substrate-nucleated pyrolytic graphite (GraphiteStore.com) that was cut to generate a 3x3 mm square of the edge plane surface. The edge plane of the graphite was utilized for all electrochemical experiments. Graphite squares were mounted onto copper wire (McMaster-Carr) using conductive silver paint (SPI) to allow for conductivity from the wire to the graphite. The wire and graphite were placed in the body of glass Pasteur pipettes (VWR) and coated in epoxy adhesive (Locktite Hysol 9460) for further stabilization of the graphite. PG electrodes were polished using a 100-grit sand paper (3M) and MilliQ water, rinsed, sonicated in fresh MilliQ water for 3 minutes at room temperature, and dried under vacuum. All reported potentials were converted to the normal hydrogen electrode (NHE) by addition of 0.198 V.

Electrochemical analysis of non-catalytic signals was performed using the SOAS program.[56] The peak positions for the FeRd anodic and cathodic peaks as a function of scan rate were determined by this program, and electroactive coverage of FeRd was obtained by integration of the anodic and cathodic peaks and calculated using Equation 2:

$$I_{int} = N_A F \upsilon \Gamma_{FeRd} \quad (2)$$

where I_{int} is the calculated integrated area of either the anodic or cathodic peak, N_A is Avogadro's number, F is Faraday's constant, ν is scan rate, and Γ_{FeRd} is the electroactive coverage. Interfacial electron transfer rates were obtained through a Laviron analysis using Butler-Volmer electron transfer theory through the JellyFit program.[30,57,58]

Quantitative Protein Film Electrochemistry (qPFE)

Quantitative protein electrochemistry was carried out as reported in Slater et al.[26] All electrochemical experiments were carried out using a 1:1 ratio of FeRd:NiRd for TOF_{app} calculations. The electroactive coverage for the FeRd was calculated as described above, and the same coverage was assumed for the NiRd. The NiRd onset potential was determined, as previously described, as the inflection point of the derivative of the cathodic segment of the CV. The capacitive current for all CVs was obtained by measuring the current at a potential 100 mV more positive than the onset of catalysis and subtracting accordingly. The current used for analysis ($i_{Eanalysis}$) was obtained at a potential 100 mV more negative than the onset of catalysis, and the apparent turnover frequency (TOF_{app}) at that analysis potential for hydrogen production by NiRd was calculated by the following equation:

$$\mathrm{TOF}_{app} = \frac{i_{E_{analysis}}}{\Gamma_{NiRd} n F} \quad (3)$$

where $i_{Eanalysis}$ is the current measured at a potential 100 mV more negative than the onset of catalysis, Γ_{NiRd} is the electroactive coverage of NiRd, n is the number of electrons (2 for H^+ reduction), and F is Faraday's constant.

The apparent turnover number (TON_{app}) is obtained from the following equation:[59]

$$\mathrm{TON}_{app} = \frac{\mathrm{TOF}_{app}}{k_{2,inact}} \quad (4)$$

where TOF_{app} is obtained from Eq. 3 and the degradation rate ($k_{2,inact}$) reflects the catalysis-induced decrease in the NiRd currents obtained from prolonged cyclic voltammetry experiments.

Electrochemical Simulations and Analysis

All electrochemical simulations were carried out as previously described.[25] All electrochemical pH and temperature dependence experiments were conducted using either CHAMP buffer at pH 4.5 or 150 mM acetate buffer, pH 4.5, at 293 K, respectively, as a buffer reference prior to subjecting each electrode to the buffer/temperature of interest. Normalized currents were calculated by dividing the measured current obtained from the buffer of interest against each reference CV obtained prior to measurement.

Absorbance Spectroscopy

All UV-visible spectra were measured using a Shimadzu UV-2600 spectrophotometer. Assessment of NiRd and FeRd stability during coupling experiments was performed by addition of all coupling regents and corresponding protein samples to a cuvette. Samples were allowed to react for 1.5 hours while monitoring the absorbance at 492 nm (FeRd) or 455 nm (NiRd).

RESULTS

Electrochemical Characterization of Covalently Attached FeRd and NiRd to Pyrolytic Graphite Electrodes

Electrochemical characterization of FeRd and NiRd on pyrolytic graphite has been previously performed utilizing protein film electrochemistry (PFE) on adsorbed protein monolayers.[25,26] Cyclic voltammograms (CVs) of adsorbed FeRd demonstrate a fully reversible Fe^{III}/Fe^{II} redox couple, while NiRd performs electrocatalytic proton reduction at modest overpotentials. While PFE is a powerful technique for electrochemical characterization of proteins, desorption of the Rd sample is observed on the timescale of minutes, compromising prolonged analysis of the catalyst as well as utility in future applications.[25] Covalent attachment of the protein to the surface of carbon-based electrodes may provide long-term stability as well as the ability to investigate changes in electron transfer and activity as a function of the distance and orientation of the enzyme active site relative to the electrode surface. In this report, Rd was attached to the electrode surface *via* carbodiimide crosslinking chemistry to form an amide bond or *via* the reaction between an aryl amine and a tyrosine residue in a Mannich-type coupling (**Scheme 1).**

For the first method, the electrode surface is modified to introduce a primary amine. This is accomplished by soaking the electrode in an aprotic solution of a nitrobenzene diazonium salt, followed by quenching with a protic solvent and electrochemical reduction of the nitro group in the presence of acid to install an aniline moiety at the surface of the electrode (**Scheme 1A**).[36] Amide coupling of an amine such as lysine to a carboxylate functional group can be accomplished by direct utilization of the oxidized surface groups present in pyrolytic graphite and

coupling to a primary amine on the protein scaffold, as shown in the directly attached electrodes (**Scheme 1B**).[50] A third approach involves introduction of a carboxylate moiety through the adsorption of a pyrene derivative onto carbon nanotubes, which are deposited on the surface of a PG electrode. The coupling reaction was then performed on the entire conductive electrode system (**Scheme 1C**).[60] In these cases, the site at which the protein is coupled to the electrode is complementary to the group on the electrode surface, either to a carboxylate side chain on the surface of the protein in the first case or to a primary amine in the latter two examples. Alternatively, a Mannich-type reaction has previously been reported for selective bond formation between a tyrosine residue and a primary aryl amine.[43] Building from this example, modification of the electrode surface as previously described for the introduction of an aniline group permits coupling of the electrode to a tyrosine residue in the protein (**Scheme 1D**). Complete electrochemical characterization of WT FeRd and WT NiRd for all coupling methods was performed to quantify the amount of protein bound to the surface and assess electron transfer efficiency (**Table 1**).

Table 1. Interfacial electron transfer parameters for WT FeRd for all coupling methods.

Coupling Method	*E° at 50 mV/s (mV vs NHE)*[a]	*k_0 (s^{-1})*	*E^{o} at 1 V/s (mV vs NHE)*[b]	*Peak separation at low scan rates (mV vs NHE)*	*Electroactive Coverage ($pmol/cm^2$)*
Adsorbed	-21 ± 7.6[c]	1020 ± 490	-17 ± 11	26 ± 3	155 ± 22
Directly Attached	+22 ± 4.2	1120 ± 88	-34 ± 13	26 ± 1	344 ± 33
Aniline Modified	+55 ± 5.5	170 ± 70	-55 ± 8	13 ± 3	100 ± 22
CNT-Pyrene	+23 ± 15	570 ± 370	-53 ± 11	34 ± 4	100 ± 11
Tyrosine Coupling	-22 ± 3.4	160 ± 70	-2 ± 10	16 ± 8	16.6 ± 10

[a]Reduction potentials obtained in 150 mM acetate buffer, pH 4.5
[b]E° values obtained from Laviron analysis on CVs run in 150 mM acetate buffer, pH 4.5, with saturated KCl
[c]Error values reflect the standard deviation from n≥3 independent experiments

Exposure of a freshly polished PG electrode surface to a solution containing protein, EDC, and NHS results in the direct, covalent attachment of the primary amine groups in rubredoxin to the carboxylate surface groups of PG electrodes via carbodiimide crosslinker chemistry.[61] The cyclic voltammogram of coupled FeRd demonstrates similar electrochemical characteristics as the ones previously reported using PFE on adsorbed protein monolayers (**Figure 2A**). The fully reversible, one-electron Fe^{III}/Fe^{II} couple is observed at -21 mV vs. NHE for the adsorbed species, while it appears at +22 mV vs. NHE for the coupled system. This reflects a shift of +43 mV upon covalent attachment. The electroactive coverages of FeRd for films generated using adsorbed and covalently attached methods were calculated using Eq. 2 to be approximately 155 ± 22 and 344 ± 33 $pmol/cm^2$, respectively. The electroactive coverage as well as the NiRd currents were also examined as a function of the coupling time (Figure S1). The FeRd surface coverage is maximized after 120 minutes of incubation with coupling reagents, while the NiRd currents appear to decrease with longer coupling times. The stability of FeRd and NiRd in the presence of coupling reagents was examined by monitoring changes in the ligand-to-metal charge transfer (LMCT) absorption bands of FeRd (492 nm) and NiRd (455 nm) as a function of time; no changes were observed in the optical spectra for FeRd over the course of 90 minutes. Minor precipitation is observed for NiRd samples, resulting in an approximately 10% decrease in the LMCT band intensity at 455 nm after removing precipitate through centrifugation (Figure S2). Importantly, the catalytic activity of NiRd is preserved upon direct covalent attachment to the PG surface using the intrinsic electrode functional groups. Moreover, this coupling method does not introduce additional reactive functionalities onto the electrode that would obscure the NiRd features. The cyclic voltammograms appear essentially identical to those measured upon adsorption of the protein to the surface, with proton reduction currents observed at an onset potential of -800 mV vs. NHE at pH 4.0, consistent with prior reports (**Figure 2A**).[26]

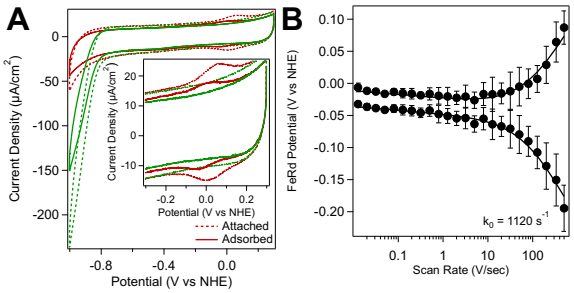

Figure 2. (**A**) Cyclic voltammogram (ν = 25 mV/s) of adsorbed (*solid lines*) and directly attached (*dashed lines*) FeRd (*red*) and NiRd (*green*) in 150 mM acetate buffer, pH 4.5. (**B**) Laviron plot and fit for cathodic and anodic peak positions of directly attached FeRd. Voltammograms were obtained in 150 mM acetate buffer, pH 4.5, with saturated KCl.

Cyclic voltammograms of Rd coupled to aniline-modified electrodes also demonstrate a fully reversible, one-electron Fe^{III}/Fe^{II} couple at +55 mV vs. NHE, with an electroactive coverage of approximately 100 $pmol/cm^2$ (Figure S3). While distinct sloping features are observed at negative potentials for FeRd and NiRd modified electrodes, NiRd electrocatalytic proton reduction currents appear generally masked due to background currents from the modified electrodes; this electrode-based proton reduction is apparent in the non-catalytic, FeRd cyclic voltammograms as well. The increased background currents appear to derive from the diazonium salt modification; electrodes prepared using this method for the Mannich-type coupling also show large currents in the negative potential region for both FeRd and NiRd (Figure S4). However, despite the NiRd signals being masked, the FeRd signals remain prominent for the tyrosine-aniline coupling approach, with the reversible, one-electron Fe^{III}/Fe^{II} couple observed at -22 mV vs. NHE and an electroactive coverage of approximately 17 $pmol/cm^2$. The CVs of CNT-pyrene modified electrodes also show a reversible, one-electron Fe^{III}/Fe^{II} couple at +23 mV vs. NHE and an electroactive coverage of approximately 100 $pmol/cm^2$ (Figure S5). However, no electrocatalytic signals for hydrogen production are observed at low potentials that can be attributed to the NiRd protein; similar traces for the attached FeRd indicate a large degree of background proton reduction by the CNTs, as previously noted.[62]

Laviron Characterization of Coupling Methods

To further investigate the impact of each coupling method on the electrode properties and protein-electrode interface, electron transfer (ET) rates for WT FeRd were assessed using a Laviron analysis.[57] The WT FeRd reduction potential shifts slightly in saturated KCl buffer, in a manner that is dependent on the method of coupling, likely reflecting a change in surface electrostatics. Interfacial electron transfer kinetics were

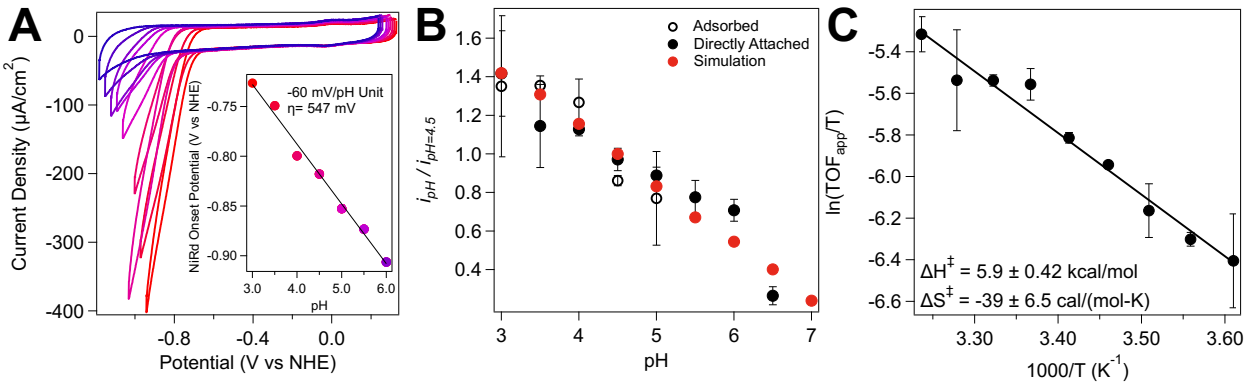

Figure 3. (**A**) Cyclic voltammograms (ν = 25 mV/s) of directly attached, 1:1 mixtures of FeRd:NiRd from pH 3 – pH 7. (***Inset***) Catalytic onset potential for NiRd as a function of pH. (**B**) NiRd currents as a function of pH normalized to those at pH 4.5 for adsorbed (*open symbols*) and attached (*closed symbols*) NiRd along with simulated pH dependence (*red*). (**C**) Temperature dependence of normalized NiRd currents with Eyring parameters indicated.

analyzed by measuring the anodic and cathodic peak potentials for the one-electron Fe^{III}/Fe^{II} redox process. As the scan rate is increased, the peak separation between the oxidative and reductive signals also increases, as has previously been seen for redox proteins in our lab and others.[30,58,63] The electron transfer parameters were determined by evaluating these peak positions in the context of Butler-Volmer electron transfer theory (**Table 1**), where k_0 reflects the electron transfer rate at zero driving force. The kinetics of interfacial electron transfer were found to depend strongly on the attachment method. Aniline-modified, carboxylate-attached electrodes exhibit an electron transfer rate of ~170 s^{-1} (Figure S3), while CNT-pyrene modified electrodes demonstrate higher electron transfer rates of around 570 s^{-1} for the reversible Fe^{III}/Fe^{II} redox couple (Figure S5). Electron transfer rates to the tyrosine-coupled FeRd are comparable to those observed for the aniline-based attachment, at 160 s^{-1}, which is unsurprising given that both methods rely on initial nitrodiazonium modification of the surface (Figure S4). Adsorption and direct covalent attachment exhibit similarly high interfacial ET rates of k_0 ~ 1020 s^{-1} and 1120 s^{-1}, respectively.

Quantitative Protein Film Electrochemistry of FeRd and NiRd

The similarity in electron transfer rates between the adsorbed and directly coupled FeRd films prompted further investigation of the NiRd voltammograms. Proton reduction currents were monitored as a function of pH and temperature to identify mechanistic changes induced by attachment to the electrode surface. Traditional electrocatalytic analyses based on the measurement of limiting currents are intractable for the study of NiRd due to the catalytic overpotential and background proton reduction in aqueous solution.[34,63] Furthermore, the absence of a non-catalytic, reversible signal for the nickel-substituted protein limits the quantification of the electroactive surface coverage for the catalyst. To overcome this limitation, we have developed and validated methodology in which the FeRd protein acts as an internal redox standard for quantifying total electroactive adsorbed protein on the electrode surface, termed quantitative protein film electrochemistry (qPFE).[26] A previous study using simple adsorption of the FeRd and NiRd proteins demonstrated the utility of this approach to identify fundamental mechanistic parameters.[26] A similar procedure was employed here to characterize the coupled system. A one-to-one ratio of Fe^{II}Rd to Ni^{II}Rd was used to obtain the FeRd coverage using Eq. 2, and the corresponding NiRd apparent turnover frequency (TOF_{app}) was obtained at a potential that is 100 mV more negative than the onset potential using Eq. 3.

The validity of extending the qPFE technique to directly coupled proteins is supported by experiments in which mixtures of FeRd and cobalt-substituted Rd (CoRd) were coupled to the electrode surface (Figure S6). Each system displays only a single, non-catalytic one-electron redox couple for which the electroactive coverage can be quantified.[26] A direct correlation between the peak area and solution concentrations is observed. Additionally, while the oxidation state of the metal impacts electroactive coverage in adsorbed mixtures of Co^{II}Rd+Fe^{III}Rd, indicating predominantly electrostatic adsorption to the surface, this limitation is not observed when the protein is directly coupled to the electrode. Instead, coupled electrodes derived from mixtures of Co^{II}Rd+Fe^{III}Rd and Co^{II}Rd+Fe^{II}Rd both show a one-to-one correlation between solution concentration and electroactive coverage. This observation further supports the utilization of this quantitative technique as a method for calculating the NiRd TOF_{app}s.

The electrocatalytic onset potential of NiRd exhibits a shift of -60 mV/pH unit, characteristic of a proton coupled electron transfer (PCET) process (**Figure 3A**).[64] Despite the shift in catalytic onset potential, the NiRd apparent turnover frequency (TOF_{app}) is effectively pH-independent between pH 3.0 – 5.0, with measured TOF values of 11 ± 0.3 s^{-1} and 34 ± 2 s^{-1} for the coupled and the adsorbed system, respectively (Figure S7). Notably, while the pH-independent rates suggest the same mechanism of proton reduction is operative, the actual values obtained for the TOF_{app}s of the covalently attached films using this qPFE analysis are approximately three-fold lower than those observed for the electrostatically adsorbed films. This discrepancy may arise from a number of factors, as discussed further below.

Covalent attachment of the protein to the electrode surface circumvents the need to study NiRd at or below the isoelectric point, expanding the experimental scope beyond pH 5. To assess the NiRd activity across this wider pH range, a different type of analysis was needed, as comparison to the adsorbed protein was no longer sufficient when examining the system above pH 5. Following the semiquantitative methodology often employed for the study of redox enzymes such as hydrogenase and

CODH,[6,34,65,66] the NiRd catalytic currents from pH 3 – 7 were considered relative to a standard, in this case, the currents at pH 4.5. A CV was obtained at pH 4.5 prior to and after obtaining the CV in the pH of interest. The current value at the appropriate analysis potential for each pH ($i_{Eanalysis}$) was divided by the average of the current values at the analysis potential for pH 4.5 (-813 mV vs NHE) to give the normalized currents ($i_{pH} / i_{pH=4.5}$; **Figure 3B**). This analysis reveals a slight dependence on pH in both the covalently attached films and the adsorbed films. Moreover, the same analysis can be performed on simulated voltammograms derived from the previously proposed CECEC mechanism for NiRd.[26] Using this mechanism and analysis procedure, the data obtained from both the adsorbed and covalently attached films demonstrate excellent agreement with the simulation.

Variable temperature electrochemical studies provide complementary mechanistic insight. An Eyring analysis reveals values for the catalytic activation enthalpy and entropy of +5.9 ± 0.42 kcal/mol and -39 ± 6.5 cal/mol-K, respectively, similar to the +9.5 ± 0.50 kcal/mol and -19.5 ± 1.0 kcal/mol previously reported for the adsorbed films (**Figure 3C**). Collectively, these data suggest that the overall mechanism of proton reduction by NiRd remains unchanged upon direct covalent attachment to the electrode surface when compared to adsorbed protein films.

Electroactive Coverage and Electron Transfer Kinetics of Lysine Mutants

The covalent attachment method presented here utilizes the surface carboxylate functional groups present in aerobically polished PG electrodes and a primary amine on the surface of the protein scaffold, supplied either by a lysine residue or the N-terminus, to form an amide bond. In order to fully characterize this type of coupling, site-directed mutagenesis was used to investigate changes in interfacial electron transfer rates relative to the distance from the coupling site to the protein active site. Five mutants were used for this study. There are two native lysine residues in WT Rd at positions 3 and 39. Each lysine was mutated to an alanine individually, generating the K03A and K39A mutants, and both lysine residues were mutated to give the K03A/K39A mutant, which has only the N-terminal amine

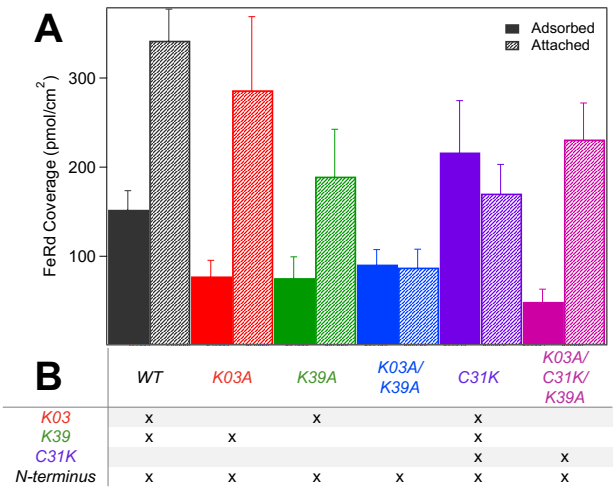

Figure 4. (**A**) Electroactive coverage of coupled (*dashed*) and adsorbed (*solid*) FeRd. (**B**) Comparison of primary amine groups present in each mutant.

group. An additional lysine residue was introduced next to the protein active site in a triple-lysine variant, C31K, and a single-lysine variant, K03A/C31K/K39A. The fold and stability of the protein were not compromised in any of the variants, as demonstrated by absorption spectra of the FeRd and NiRd variants (Figure S8). Each mutant was coupled to the surface of PG electrodes in the same manner as WT, and the electron transfer kinetics were studied through a Laviron analysis (Figure S9). As observed in WT FeRd, the electron transfer rates for each mutant did not differ significantly between the direct coupling and adsorption methods. Moreover, the rates of each mutant were similar to one another, with $k_0 \sim 1000\ s^{-1}$, indicating that the ET kinetics are mostly unaffected by changes in the location of the attachment site. The only mutant to show deviation from these rates is C31K, though the difference in ET kinetics is minor.

The electroactive coverage for each of the FeRd mutants was also examined for both the adsorbed and covalently attached protein films (**Figure 4A**). Covalent attachment of WT FeRd to the electrode surface increases the electroactive coverage by a factor of two relative to simple adsorption methods, as mentioned above; this trend is also observed across almost all of the Rd mutants. Decreased coverage is seen for directly coupled mutants that lack the K39 residue, suggesting the coupling sites are dominated by either the protein N-terminus or K39 (**Figure 4B**). In our hands, attempts to selectively acetylate the N-terminus in the K03A/K39A NiRd mutant resulted in irreversible loss of metal, precluding isolation of the contribution from just K39.

Prolonged Protein Stability Following Modification

Desorption of proteins both during catalysis and in the absence of applied potential is one of the primary disadvantages of simple adsorption methods.[35] To investigate the impact of covalent attachment on long-term protein film stability, directly coupled FeRd and NiRd were examined during extended timescale electrochemical experiments as well as after storage of the modified electrodes. Directly attached Rd demonstrates excellent stability, as indicated by both the NiRd catalytic currents and the FeRd non-catalytic features throughout an extensive repeated cyclic voltammogram experiment (**Figure 5**, Figure S10). This stability can be directly compared to that of adsorbed Rd. The NiRd current profiles decay exponentially with two characteristic rate constants of approximately $k_{1,inact} = 0.373 \times 10^{-3}\ s^{-1}$ and $k_{2,inact} = 4.46 \times 10^{-3}\ s^{-1}$ for the adsorbed species and $k_{1,inact} = 0.167 \times 10^{-3}\ s^{-1}$ and $k_{2,inact} = 1.64 \times 10^{-3}\ s^{-1}$ for the covalently attached species. The peak currents for the covalently attached FeRd were also measured as a function of time and found to decay monoexponentially, giving a characteristic rate constant of approximately $k_{FeRd} = 0.275 \times 10^{-3}\ s^{-1}$. The stability towards storage of the covalently attached Rd electrodes was also examined. Electrodes that contained an equal ratio of FeRd and NiRd were stored for several weeks at 4˚C in 50 mM Tris buffer, pH 8.0, and tested periodically (**Figure 5C**). Electrochemical signals from both the Fe^{III}/Fe^{II} redox couple and NiRd catalysis were observed to persist for over 25 days, with only a 50% decrease in FeRd coverage and a 77% decrease in NiRd catalytic currents over that timeframe.

DISCUSSION

Direct Coupling to the Electrode Surface is the Preferred Covalent Attachment Method for Rubredoxin

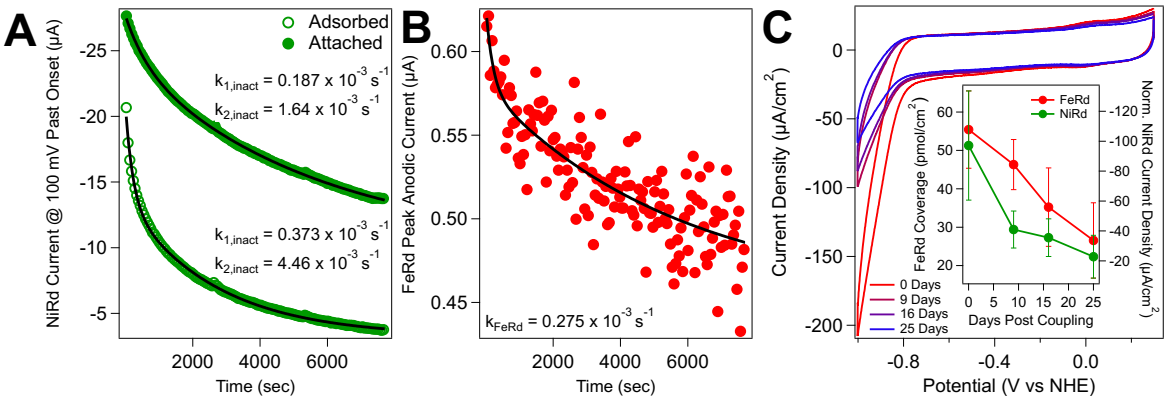

Figure 5. Stability of attached Rd films over time. (**A**) Catalytic currents of directly attached (*closed symbols*) and adsorbed (*open symbols*) NiRd and (**B**) non-catalytic currents of directly attached FeRd upon prolonged electrolysis. Best-fit lines to exponential functions shown (*black*) with characteristic rate constants indicated on figure. (**C**) Representative cyclic voltammograms of covalently attached, 1:1 mixtures of WT FeRd:NiRd over time. (***Inset***) FeRd electroactive coverage (*left*) and NiRd normalized current (*right*) over time. All CVs were measured in 150 mM acetate buffer, pH 4.5, ν = 25 mV/s.

The electrochemical characterization of adsorbed protein monolayers onto carbon-based electrodes has been widely utilized as a tool to study redox proteins and enzymes.[34,65] While powerful in its simplicity and general applicability, this technique is limited by the strength of the protein-surface interaction. Additionally, the catalytic currents are dependent both upon the enzyme activity and the adsorption interaction, rendering it particularly difficult to disentangle the effects of interfacial electron transfer, film stability, and inherent activity. Extensive characterization of the electrochemical properties of surface-adsorbed FeRd and NiRd has been previously reported.[25,26,28] In this work, diverse methods to covalently attach the protein to the surface of the electrode have been applied to increase the stability of the protein on the electrode surface and study orientation and distance effects on electron transfer and electrocatalysis, as well as investigate whether covalent attachment changes the proton reduction mechanism. Though extensive methodology has been developed in recent years to covalently attach redox-active systems to the surfaces of electrodes, these modifications, either to the protein or the electrode surface, often result in increased background reactivity from the electrode or denaturation of the protein.[33] These undesired effects were also observed for the Rd system. For instance, while pyrene derivatives adsorbed to CNT-coated surfaces are widely utilized as means to stabilize proteins on the surface of electrodes as well as achieve higher protein coverage on the surface, it was difficult to observe electrocatalysis upon attachment of NiRd (Figure S5). The addition of CNTs increases the capacitive current of the electrode, likely due to the formation of several CNT layers, and CNTs themselves are reactive at low potentials, which in turn obscures the catalytic signal of NiRd at negative potentials. A similar result is obtained from aniline modified electrodes,[41] which results in highly reactive electrodes at negative potentials that dominate over the NiRd electrocatalytic signals (Figure S3).

Due to these issues, we have taken advantage of the existing carboxylate-containing functional groups at the surface of pyrolytic graphite.[52] This approach eliminates background currents from the tethering moiety and provides optimal covalent attachment of both FeRd and NiRd to a PG surface. Using carbodiimide crosslinking chemistry, the protein was successfully attached to the surface of the electrode through amine functional groups, as observed electrochemically (**Figure 2A**). Similar rates of electron transfer for the adsorbed and covalently attached WT FeRd are observed, as no orientation selection is employed nor are additional linkers between the surface of the electrode and the protein installed. The electroactive coverage of the coupled FeRd increases by approximately two-fold relative to that seen for simple adsorption, demonstrating effective utilization of the electrode surface. It is important to note that the reported coverage numbers are only indicative of the electroactive protein on the surface of the electrode. Electrochemically inactive protein may also occupy the surface of the electrode, contributing to the capacitive but not the faradaic currents; this interference is possible for both covalently attached and adsorbed electrodes.

In addition to electrochemical characterization of the FeRd system, the catalytic activity of covalently attached NiRd was assessed. Consistent with the minor shift in potential observed for the $Fe^{III/II}$Rd redox couple (Figure S11), the overpotential for catalysis from pH 3 – 5 is unchanged for the attached protein relative to the adsorbed protein. However, rapid decreases in current due to desorption or inactivation are not observed during the duration of the cyclic voltammetry experiment. Moreover, the catalytic activity of NiRd can be evaluated at pH values greater than 5, measurements that are not possible using simple adsorption due to electrostatic repulsion above the pI of the protein. From these experiments, NiRd activity appears to be limited at pH values greater than 7, though transfer of that same electrode to a lower pH buffer restores catalysis (**Figure 3A**; Figure S12). The capacitive current of the electrode throughout the experiment remains constant, reducing the likelihood that irreversible degradation is responsible for the lack of activity at higher pH values.

The catalytic onset potential and pH dependence of NiRd activity for the other covalent attachment methods were also characterized. While NiRd signals for the aniline modified electrode were similar to those observed for directly coupled electrodes (Figure S13-S14), the catalytic signals for NiRd were largely masked by background currents of the CNTs adsorbed onto the electrode (Figure S15-S16). The tyrosine-based coupling strategy resulted in visible voltammetric signals for FeRd, but

unfortunately, the background currents from the modified electrode masked the characteristic linear catalytic waveshape of the NiRd activity (Figure S17). Moreover, only low coverage was observed for the reversible FeRd signals.

Quantitative protein film electrochemistry of covalently attached FeRd and NiRd indicates the mechanism of catalysis is unchanged but the elementary rate constants may be affected

Having demonstrated the successful attachment and preservation of electrochemical activity of both FeRd and NiRd, quantitative protein film electrochemistry was used to study the mechanism of catalysis for the coupled films, analogous to previously reported work on adsorbed Rd films. The calculated TOF_{app}s for hydrogen production of covalently attached NiRd, analyzed using the qPFE method, are approximately three-fold lower than that of the adsorbed system, though the constant values observed from pH 3- 5 suggests that the overall mechanism in this pH range remains unaffected (Figure S7).[26] Reduced dynamics of the protein upon covalent attachment may contribute to the decreased activity of the enzyme, as has previously been reported for small molecule complexes when attached to electrode surfaces.[67] A recent combined electrochemical, crystallographic, and computational study on a library of NiRd mutants has suggested that dynamics of the protein are critical for catalysis, with mutants exhibiting greater flexibility around the active site demonstrating turnover frequencies that are 10-fold greater than WT NiRd.[28] This has been attributed to increased transient substrate accessibility, necessary for proton binding; additionally, because the rate-determining step has previously been suggested to be intramolecular proton transfer through thiol inversion, restricted dynamics could substantially impact this process.

Electrochemical simulations of the catalytic current as a function of pH were previously used to constrain the mechanism of H_2 evolution by adsorbed NiRd (**Figure 6**).[26] These simulations quantitatively agreed with experiment and allowed the extraction of intrinsic rate constants and thermodynamic parameters associated with catalysis, such as the pK_a associated with the initial protonation step in the CECEC mechanism (~2.5) and the inherent reduction potential of NiRd (-0.752 V vs. NHE). This analysis was used in conjunction with kinetic isotope effects and computational studies to suggest that the rate-determining

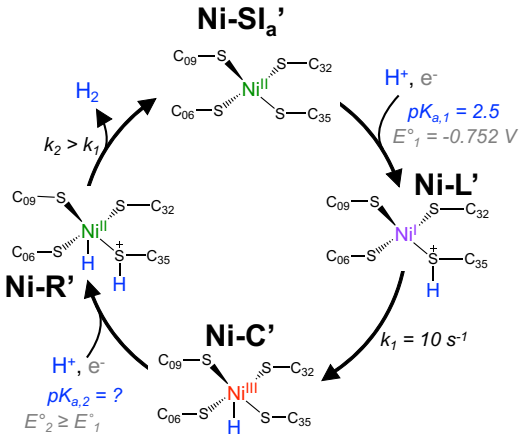

Figure 6. Proposed catalytic mechanism and key parameters for covalently-attached nickel-substituted rubredoxin.

step for catalysis is intramolecular proton transfer from a Ni^{I}-SH species to form a Ni^{III}-H state, which, in the adsorbed WT NiRd, occurs with a $k_1 \sim 130\ s^{-1}$. The subsequent reduction and protonation steps are unresolved within this model. The lower TOF_{app}s observed for the covalently attached system were investigated using voltammetric simulations to establish which parameters might be impacted. At fast scan rates, a small non-catalytic signal is recovered that can be modeled with a Laviron-type analysis, giving an interfacial ET rate, k_0, of ~125 s^{-1} (Figure S18). This is comparable to the rate obtained for the adsorbed system ($k_0 \sim 75\ s^{-1}$), suggesting decreased ET rates are not the dominant factor contributing to the lower activity. Simulations support this analysis, as decreasing the electron transfer rate has only negligible effect on the expected catalytic currents or TOF_{app}s (Figure S19). Varying the pK_a is also not sufficient to reproduce the lower activity, instead predominantly affecting the onset potential and pH dependence (Figure S20). Only decreasing the rate constant for the intramolecular chemical step, k_1, gives a lowered TOF_{app} but retains the pH profile for the absolute and relative activity (Figure S21). Good agreement with experiment and simulation is observed when k_1 for the attached species is decreased by approximately an order of magnitude to ~10 s^{-1}. This process is modeled as an intramolecular proton transfer step, which requires flexibility of the protein active site loops and backbone. Considering the likelihood of restricted motion upon covalent attachment to the electrode surface, this modest change to the catalytic parameters seems feasible.

In support of this suggestion, an Eyring analysis of variable temperature electrochemical experiments performed at pH 4.5 revealed a negative entropy of activation for the covalently attached system that is approximately two-fold greater in magnitude than that measured for the adsorbed system. A large, negative entropy of activation is consistent with an ordered transition state, such as that in which thiol inversion is the rate determining step, as the transition state has been calculated to fall directly between the Ni^{I}-SH and Ni^{III}-H species and thus would involve a three-center, two-electron type of configuration (**Figure 6**).[26] Using these parameters, the free energy of activation ($\Delta G^{\neq}$) is calculated to be 17.3 ± 1.9 kcal/mol at 293 K. This is greater than that obtained for the adsorbed system, which was calculated to be 14.7 ± 0.6 kcal/mol. Using a simple Arrhenius estimation, this ~2.6 kcal/mol increase in $\Delta G^{\neq}$ should result in a decrease in rate of a factor of ~80, greater than the 10-fold decrease observed, though the large degree of error observed and exponential dependence of the rates on $\Delta G^{\neq}$ renders this analysis necessarily approximate.

As a complementary approach to the qPFE analysis, the catalytic current at pH 4.5 was used as a point of normalization to obtain a relative activity profile. This methodology is commonly used for studying native hydrogenases along with other redox enzymes for which substrate control or non-catalytic waves cannot easily be accessed. Excellent agreement was obtained for the normalized currents of attached and adsorbed films as well as with the simulation (**Figure 3B**).

While the qPFE results and electrochemical simulations suggest restricted dynamics and/or substrate accessibility are responsible for the decreased activity, another explanation that would be consistent with the experimental data is that the absolute electroactive coverage of the attached NiRd is overestimated, or a larger fraction of NiRd is inactive relative to the adsorbed system. While solution-phase control experiments demonstrate that NiRd is stable under the coupling conditions

when performed in solution (Figure S2), and experiments with mixtures of CoRd and FeRd in different oxidation states suggest that the amount of protein that attaches is independent of metal identity (Figure S6), it has previously been shown in a cytochrome c peroxidase enzyme that electrocatalytic activity differs from the amount of non-catalytic redox signal observed.[68] Thus, we consider that the assumptions previously made and validated for the qPFE analysis of adsorbed films may not all be valid for the covalently attached system. Ongoing and future *in situ* spectroelectrochemical studies will be allow us to identify which of these possibilities is responsible for the lowered NiRd catalytic currents.

Only Minor Changes in Electroactive Coverage and Electron Transfer Kinetics are observed as a Function of Coupling Site

Targeted mutations were introduced in order to interrogate the electron transfer rates and electroactive coverage as the number and location of coupling sites were changed. Perturbing the distance between the surface and the protein active site may impact the protein dynamics at the surface, which can be probed through analysis of ET kinetics and relative catalytic currents. The adsorbed electroactive coverage across all mutants reflects the overall charge on the system, as the C31K mutant, which has a net +2 charge relative to WT, shows increased adsorption, and each of the single-lysine mutants has approximately half the coverage of WT FeRd. This is consistent with electrostatic attraction between the negatively charged electrode surface and the positively charged protein as the dominant interaction. On the other hand, the two lysine residues do not seem to affect covalent attachment in the same manner. The electroactive coverage of the WT, K03A, and C31K mutants are all approximately the same, suggesting that the K03 residue does not play a substantial role in coupling the protein to the electrode. On the other hand, the K39A and K03A/K39A mutants show approximately 50% decrease in coverage, indicating that the N-terminus of the protein and the K39 residue contribute equally to the coupling reaction. The intermediate coverage observed for the triple mutant, K03A/C31K/K39A, over the K03A/K39A mutant seems to indicate a relatively small contribution of C31K as a site for electrode attachment.

Surprisingly, the interfacial ET kinetics are also relatively insensitive to the coupling site, as no obvious correlation between ET rate and the distance from the electrode is observed. For example, the K03 site and N-terminus are approximately 15-20 Å from the metal center, according to the crystal structure of NiRd (PDB 6NW0), while the C31K site is immediately adjacent to the C32 metal-binding residue. Within error, there is no significant difference in peak-to-peak separation as a function of scan rate between the K39A and the triple mutants, suggesting that the interfacial ET rate is not dominated by through-space distance between the electrode attachment site and the metal center. This is likely due to the small size of Rd as well as the flexibility of the lysine-based attachment site, which may permit the metal center to approach the electrode with approximately the same distance across all of the constructs.

Protein and Electrode Stability is Extended Significantly through Covalent Attachment

A particularly exciting feature of the described direct attachment method is the prolonged stability of the enzyme on the surface of the electrode. Directly coupled NiRd and FeRd are stable not only during extended electrolysis but also upon storage for many days; the surface-attached NiRd electrocatalytic signal is still observed 25 days after coupling (**Figure 5**). While this is not necessarily surprising for FeRd, which is an electron transfer protein, artificial enzymes are not generally known for robustness. This degree of stability is unprecedented for Rd on electrodes and overcomes one of the major challenges of bioelectrocatalysis.[3] Thus, simple but effective direct attachment to inexpensive electrode surfaces may offer opportunities for further optimization of NiRd and ultimate utilization in industrial applications.

The protein decay also appears to depend on whether the electrode is under applied potential. Continuous electrolysis in the form of cyclic voltammograms run over the timescale of 2 hours suggest two mechanisms of decay for NiRd, as the current decrease follows a biexponential function. The FeRd signals, on the other hand, decrease monoexponentially. The lower rate constant ($k_{1,inact}$) of the covalently attached NiRd (0.187×10^{-3} s^{-1}) is similar to that of FeRd ($k_{FeRd} = 0.275 \times 10^{-3}$ s^{-1}), suggesting that this decrease derives from the same degradation mechanism. This may reflect the inherent denaturation of the protein fold under extended exposure to high local electric fields, a phenomenon that has previously been observed for urease and myoglobin, nickel and iron proteins, respectively.[69,70]

An additional, more rapid process with a rate constant ($k_{2,inact}$) of approximately 1.64×10^{-3} s^{-1} is observed only for NiRd and is attributed to decay pathways accessible during catalysis. As the NiRd enzyme is expected to proceed through multiple distinct intermediates during turnover, it is considered feasible that a degradative side reaction could occur within any of these states. By considering the relative rates of turnover at pH 4.0 ($TOF_{app} = 11$ s^{-1}) and the catalysis-induced degradation rate $k_{2,inact}$, an apparent turnover number (TON_{app}) for NiRd is estimated at 6700 (Eq. 4).[59] This TON_{app} reflects the branching ratio for the likelihood of NiRd proceeding through productive vs. unproductive pathways. In support of this analysis, the rate of decay of the catalytic signal, $k_{2,inact}$, that can be attributed to turnover for adsorbed NiRd is approximately three-fold higher than that of the covalently attached enzyme. However, the TOF_{app}, as estimated by the qPFE method, is also three-fold higher for the adsorbed system. Thus, the branching ratio for catalysis relative to degradation remains approximately the same, and the TON_{app} is estimated from Eq. 4 to be 7600. That similar and high TONs are observed for adsorbed and covalently attached NiRd further indicates that a similar catalytic mechanism is followed in both systems. Future work will couple NiRd electrolysis to gas chromatography measurements as a function of potential in order to gain information on the mechanism(s) of decay, which will offer a route for further rational optimization.

CONCLUSIONS

Artificial metalloenzymes offer promise for reproducing the high activities and efficiencies of native enzymes. In this work, the optimal attachment of a model hydrogenase enzyme, nickel-substituted rubredoxin (NiRd), to carbon-based electrodes is shown to rely on direct coupling to the surface carboxylate functional groups. The resultant electrode system is stable for H_2 evolution for a period of several weeks, with high estimated turnover numbers of ~6700. While the absolute turnover frequencies are lower for the attached enzyme, electrochemical simulations reveal that the dominant change is in the rate of the intramolecular proton transfer step, highlighting the importance

of dynamics in catalysis. This simple but effective methodology can broadly be applied to the study of many different redox-active metalloproteins and enzymes across diverse reaction conditions. Moreover, the extended stability observed for these simple and inexpensive electrodes suggests potential application of nickel-substituted rubredoxin for effecting prolonged electrocatalytic hydrogen evolution under benign reaction conditions.

ASSOCIATED CONTENT

Supporting Information

Detailed materials and methods, supplemental figures presenting detailed work-up protocols, optical spectra, and electrochemical simulations.

The Supporting Information is available free of charge on the ACS Publications website.

AUTHOR INFORMATION

Corresponding Author

*shafaat.1@osu.edu

Present Addresses

†Current address: Department of Chemistry, The Pennsylvania State University, University Park, PA 16802, USA.

Author Contributions

The manuscript was written through contributions of all authors. All authors have given approval to the final version of the manuscript.

Funding Sources

This work was supported by the U.S. National Science Foundation (CHE-1454289).

Notes

Any additional relevant notes should be placed here.

ACKNOWLEDGMENTS

H.S.S. would like to acknowledge the National Science Foundation (CHE-1454289) for support of this work. R.E.T. would like to acknowledge the Department of Education for a GAANN graduate fellowship. We also gratefully acknowledge helpful feedback, advice, and mentorship from Deborah Zamble and want to recognize her significant contributions to the hydrogenase field.

ABBREVIATIONS

Rd, rubredoxin; NiRd, nickel-substituted rubredoxin; PG, pyrolytic graphite; CV, cyclic voltammetry; TOF_{app}, apparent turnover frequency; TON_{app}, apparent turnover number; qPFE, quantitative protein film voltammetry.

REFERENCES

(1) Turner, J. A. Sustainable Hydrogen Production. *Science* **2004**, *305*, 972–974.

(2) Armstrong, F. A.; Hirst, J. Reversibility and efficiency in electrocatalytic energy conversion and lessons from enzymes. *PNAS* **2011**, *108*, 14049–14054.

(3) Rasmussen, M.; Abdellaoui, S.; Minteer, S. D. Enzymatic biofuel cells: 30 years of critical advancements. *Biosensors and Bioelectronics* **2016**, *76*, 91–102.

(4) Reisner, E. Solar Hydrogen Evolution with Hydrogenases: From Natural to Hybrid Systems. *Eur. J. Inorg. Chem.* **2011**, No. 7, 1005–1016.

(5) Lubitz, W.; Ogata, H.; Rüdiger, O.; Reijerse, E. Hydrogenases. *Chem. Rev.* **2014**, *114*, 4081–4148.

(6) Armstrong, F. A.; Evans, R. M.; Hexter, S. V.; Murphy, B. J.; Roessler, M. M.; Wulff, P. Guiding Principles of Hydrogenase Catalysis Instigated and Clarified by Protein Film Electrochemistry. *Acc. Chem. Res.* **2016**, *49*, 884–892.

(7) Shafaat, H. S.; Rüdiger, O.; Ogata, H.; Lubitz, W. [NiFe] hydrogenases: A common active site for hydrogen metabolism under diverse conditions. *Biochim. Biophys. Acta-Bioenerg.* **2013**, *1827*, 986–1002.

(8) Adamson, H.; Robinson, M.; Wright, J. J.; Flanagan, L. A.; Walton, J.; Elton, D.; Gavaghan, D. J.; Bond, A. M.; Roessler, M. M.; Parkin, A. Retuning the Catalytic Bias and Overpotential of a [NiFe]-Hydrogenase via a Single Amino Acid Exchange at the Electron Entry/Exit Site. *J. Am. Chem. Soc.* **2017**, *139*, 10677–10686.

(9) Artz, J. H.; Zadvornyy, O. A.; Mulder, D. W.; Keable, S. M.; Cohen, A. E.; Ratzloff, M. W.; Williams, S. G.; Ginovska, B.; Kumar, N.; Song, J.; McPhillips, S. E.; Davidson, C.; Lyubimov, A. Y.; Pence, N.; Schut, G. J.; Jones, A. K.; Soltis, S. M.; Adams, M.; Raugei, S.; King, P. W.; Peters, J. W. Tuning catalytic bias of hydrogen gas producing hydrogenases. *J. Am. Chem. Soc.* **2020**, *142*, 1227–1235.

(10) Fourmond, V.; Wiedner, E. S.; Shaw, W. J.; Léger, C. Understanding and Design of Bidirectional and Reversible Catalysts of Multielectron, Multistep Reactions. *J. Am. Chem. Soc.* **2019**, *141*, 11269–11285.

(11) Lansing, J. C.; Manor, B. C.; Rauchfuss, T. B. Hydrogenase Models. In *Encyclopedia of Inorganic and Bioinorganic Chemistry*; John Wiley & Sons, Ltd, 2011.

(12) Bethel, R. D.; Darensbourg, M. Y. The Bioorganometallic Chemistry of Hydrogenase. In *Bioorganometallic Chemistry*; Jaouen, G., Salmain, M., Eds.; Wiley-VCH Verlag GmbH & Co. KGaA, 2014; pp 239–272.

(13) Dutta, A.; Appel, A. M.; Shaw, W. J. Designing electrochemically reversible H 2 oxidation and production catalysts. *Nat. Rev. Chem.* **2018**, *2*, 244.

(14) Ginovska-Pangovska, B.; Dutta, A.; Reback, M. L.; Linehan, J. C.; Shaw, W. J. Beyond the Active Site: The Impact of the Outer Coordination Sphere on Electrocatalysts for Hydrogen Production and Oxidation. *Acc. Chem. Res.* **2014**, *47*, 2621–2630.

(15) Brooke, E. J.; Evans, R. M.; Islam, S. T. A.; Roberts, G. M.; Wehlin, S. A. M.; Carr, S. B.; Phillips, S. E. V.; Armstrong, F. A. Importance of the Active Site "Canopy" Residues in an O2-Tolerant [NiFe]-Hydrogenase. *Biochemistry* **2017**, *56*, 132–142.

(16) Jeong, W. J.; Yu, J.; Song, W. J. Proteins as diverse, efficient, and evolvable scaffolds for artificial metalloenzymes. *Chem. Commun.* **2020**, *56*, 9586–9599.

(17) Mirts, E. N.; Petrik, I. D.; Hosseinzadeh, P.; Nilges, M. J.; Lu, Y. A designed heme-[4Fe-4S] metalloenzyme catalyzes sulfite reduction like the native enzyme. *Science* **2018**, *361*, 1098–1101.

(18) Selvan, D.; Prasad, P.; Farquhar, E. R.; Shi, Y.; Crane, S.; Zhang, Y.; Chakraborty, S. Redesign of a Copper Storage Protein into an Artificial Hydrogenase. *ACS Catal.* **2019**, *9*, 5847–5859.

(19) Jenney, F. E.; Adams, M. W. W. [5] Rubredoxin from Pyrococcus furiosus. In *Methods in Enzymology*; Elsevier, 2001; Vol. 334, pp 45–55.

(20) Saint-Martin, P.; Lespinat, P. A.; Fauque, G.; Berlier, Y.; LeGall, J.; Moura, I.; Teixeira, M.; Xavier, A. V.; Moura, J. J. Hydrogen production and deuterium-proton exchange reactions catalyzed by Desulfovibrio nickel (II)-substituted rubredoxins. *Proc. Natl. Acad. Sci. U. S. A.* **1988**, *85*, 9378–9380.

(21) Moura, I.; Teixeira, M.; Legall, J.; Moura, J. J. G. Spectroscopic Studies of Cobalt and Nickel-Substituted Rubredoxin and Desulforedoxin. *J. Inorg. Biochem.* **1991**, *44*, 127–139.

(22) Thapper, A.; Rizzi, A. C.; Brondino, C. D.; Wedd, A. G.; Pais, R. J.; Maiti, B. K.; Moura, I.; Pauleta, S. R.; Moura, J. J. G.

Copper-substituted forms of the wild type and C42A variant of rubredoxin. *J. Inorg. Biochem.* **2013**, *127*, 232–237.
(23) Maiti, B. K.; Maia, L. B.; Silveira, C. M.; Todorovic, S.; Carreira, C.; Carepo, M. S. P.; Grazina, R.; Moura, I.; Pauleta, S. R.; Moura, J. J. G. Incorporation of molybdenum in rubredoxin: models for mononuclear molybdenum enzymes. *J Biol Inorg Chem* **2015**, *20*, 821–829.
(24) Ogata, H.; Nishikawa, K.; Lubitz, W. Hydrogens detected by subatomic resolution protein crystallography in a [NiFe] hydrogenase. *Nature* **2015**, *520*, 571–574.
(25) Slater, J. W.; Shafaat, H. S. Nickel-Substituted Rubredoxin as a Minimal Enzyme Model for Hydrogenase. *J. Phys. Chem. Lett.* **2015**, *6*, 3731–3736.
(26) Slater, J. W.; Marguet, S. C.; Monaco, H. A.; Shafaat, H. S. Going beyond Structure: Nickel-Substituted Rubredoxin as a Mechanistic Model for the [NiFe] Hydrogenases. *J. Am. Chem. Soc.* **2018**, *140*, 10250–10262.
(27) Slater, J. W.; Marguet, S. C.; Cirino, S. L.; Maugeri, P. T.; Shafaat, H. S. Experimental and DFT Investigations Reveal the Influence of the Outer Coordination Sphere on the Vibrational Spectra of Nickel-Substituted Rubredoxin, a Model Hydrogenase Enzyme. *Inorg. Chem.* **2017**, *56*, 3926–3938.
(28) Slater, J. W.; Marguet, S. C.; Gray, M. E.; Monaco, H. A.; Sotomayor, M.; Shafaat, H. S. Power of the Secondary Sphere: Modulating Hydrogenase Activity in Nickel-Substituted Rubredoxin. *ACS Catal.* **2019**, *9*, 8928–8942.
(29) Armstrong, F. A.; Belsey, N. A.; Cracknell, J. A.; Goldet, G.; Parkin, A.; Reisner, E.; Vincent, K. A.; Wait, A. F. Dynamic electrochemical investigations of hydrogen oxidation and production by enzymes and implications for future technology. *Chemical Society Reviews* **2009**, *38*, 36–51.
(30) Jeuken, L. J.; Armstrong, F. A. Electrochemical origin of hysteresis in the electron-transfer reactions of adsorbed proteins: contrasting behavior of the "blue" copper protein, azurin, adsorbed on pyrolytic graphite and modified gold electrodes. *J. Phys. Chem. B* **2001**, *105*, 5271–5282.
(31) Fujita, K.; Nakamura, N.; Ohno, H.; Leigh, B. S.; Niki, K.; Gray, H. B.; Richards, J. H. Mimicking protein-protein electron transfer: Voltammetry of Pseudomonas aeruginosa azurin and the Thermus thermophilus Cu-A domain at omega-derivatized self-assembled-monolayer gold electrodes. *J. Am. Chem. Soc.* **2004**, *126*, 13954–13961.
(32) Blanford, C. F.; Armstrong, F. A. The pyrolytic graphite surface as an enzyme substrate: microscopic and spectroscopic studies. *J. Solid State Electrochem.* **2006**, *10*, 826–832.
(33) Milton, R. D.; Minteer, S. D. Direct enzymatic bioelectrocatalysis: differentiating between myth and reality. *J. R. Soc. Interface* **2017**, *14*, 20170253.
(34) Léger, C.; Jones, A. K.; Roseboom, W.; Albracht, S. P. J.; Armstrong, F. A. Enzyme Electrokinetics: Hydrogen Evolution and Oxidation by Allochromatium vinosum [NiFe]-Hydrogenase†. *Biochemistry* **2002**, *41*, 15736–15746.
(35) Fourmond, V.; Lautier, T.; Baffert, C.; Leroux, F.; Liebgott, P.-P.; Dementin, S.; Rousset, M.; Arnoux, P.; Pignol, D.; Meynial-Salles, I.; Soucaille, P.; Bertrand, P.; Léger, C. Correcting for Electrocatalyst Desorption and Inactivation in Chronoamperometry Experiments. *Anal. Chem.* **2009**, *81*, 2962–2968.
(36) Rüdiger, O.; Abad, J. M.; Hatchikian, E. C.; Fernandez, V. M.; De Lacey, A. L. Oriented immobilization of Desulfovibrio gigas hydrogenase onto carbon electrodes by covalent bonds for nonmediated oxidation of H2. *J. Am. Chem. Soc.* **2005**, *127*, 16008–16009.
(37) Alonso-Lomillo, M. A.; Rüdiger, O.; Maroto-Valiente, A.; Velez, M.; Rodríguez-Ramos, I.; Muñoz, F. J.; Fernández, V. M.; De Lacey, A. L. Hydrogenase-Coated Carbon Nanotubes for Efficient H2 Oxidation. *Nano Lett.* **2007**, *7*, 1603–1608.
(38) Rüdiger, O.; Gutiérrez-Sánchez, C.; Olea, D.; Pereira, I. A. C.; Vélez, M.; Fernández, V. M.; De Lacey, A. L. Enzymatic Anodes for Hydrogen Fuel Cells based on Covalent Attachment of Ni-Fe Hydrogenases and Direct Electron Transfer to SAM-Modified Gold Electrodes. *Electroanalysis* **2010**, *22*, 776–783.
(39) Milton, R. D.; Wang, T.; Knoche, K. L.; Minteer, S. D. Tailoring Biointerfaces for Electrocatalysis. *Langmuir* **2016**, *32*, 2291–2301.
(40) Ash, P. A.; Vincent, K. A. Spectroscopic analysis of immobilised redox enzymes under direct electrochemical control. *Chem. Commun.* **2012**, *48*, 1400–1409.
(41) Allongue, P.; Delamar, M.; Desbat, B.; Fagebaume, O.; Hitmi, R.; Pinson, J.; Savéant, J.-M. Covalent Modification of Carbon Surfaces by Aryl Radicals Generated from the Electrochemical Reduction of Diazonium Salts. *J. Am. Chem. Soc.* **1997**, *119*, 201–207.
(42) Evrard, D.; Lambert, F.; Policar, C.; Balland, V.; Limoges, B. Electrochemical Functionalization of Carbon Surfaces by Aromatic Azide or Alkyne Molecules: A Versatile Platform for Click Chemistry. *Chem. Eur. J.* **2008**, *14*, 9286–9291.
(43) Joshi, N. S.; Whitaker, L. R.; Francis, M. B. A Three-Component Mannich-Type Reaction for Selective Tyrosine Bioconjugation. *J. Am. Chem. Soc.* **2004**, *126*, 15942–15943.
(44) Kariuki, J. K.; McDermott, M. T. Formation of Multilayers on Glassy Carbon Electrodes via the Reduction of Diazonium Salts. *Langmuir* **2001**, *17*, 5947–5951.
(45) Gentil, S.; Lalaoui, N.; Dutta, A.; Nedellec, Y.; Cosnier, S.; Shaw, W. J.; Artero, V.; Le Goff, A. Carbon-Nanotube-Supported Bio-Inspired Nickel Catalyst and Its Integration in Hybrid Hydrogen/Air Fuel Cells. *Angew. Chem. Int. Ed.* **2017**, *56*, 1845–1849.
(46) Lojou, É.; Luo, X.; Brugna, M.; Candoni, N.; Dementin, S.; Giudici-Orticoni, M. T. Biocatalysts for fuel cells: efficient hydrogenase orientation for H2 oxidation at electrodes modified with carbon nanotubes. *J Biol Inorg Chem* **2008**, *13*, 1157–1167.
(47) Bahr, J. L.; Yang, J.; Kosynkin, D. V.; Bronikowski, M. J.; Smalley, R. E.; Tour, J. M. Functionalization of Carbon Nanotubes by Electrochemical Reduction of Aryl Diazonium Salts: A Bucky Paper Electrode. *J. Am. Chem. Soc.* **2001**, *123*, 6536–6542.
(48) Banks, C. E.; Compton, R. G. New electrodes for old: from carbon nanotubes to edge plane pyrolytic graphite. *Analyst* **2006**, *131*, 15–21.
(49) Goff, A. L.; Moggia, F.; Debou, N.; Jegou, P.; Artero, V.; Fontecave, M.; Jousselme, B.; Palacin, S. Facile and tunable functionalization of carbon nanotube electrodes with ferrocene by covalent coupling and π-stacking interactions and their relevance to glucose bio-sensing. *J. Electroanal. Chem.* **2010**, *641*, 57–63.
(50) Wildgoose, G. G.; Abiman, P.; Compton, R. G. Characterising chemical functionality on carbon surfaces. *J. Mater. Chem.* **2009**, *19*, 4875–4886.
(51) Marchesan, S.; Prato, M. Under the lens: carbon nanotube and protein interaction at the nanoscale. *Chem. Commun.* **2015**, *51*, 4347–4359.
(52) Banks, C. E.; Compton, R. G. Edge plane pyrolytic graphite electrodes in electroanalysis: an overview. *Anal. Sci.* **2005**, *21*, 1263–1268.
(53) Jackson, M. N.; Oh, S.; Kaminsky, C. J.; Chu, S. B.; Zhang, G.; Miller, J. T.; Surendranath, Y. Strong Electronic Coupling of Molecular Sites to Graphitic Electrodes via Pyrazine Conjugation. *J. Am. Chem. Soc.* **2018**, *140*, 1004–1010.
(54) Manesis, A. C.; Musselman, B. W.; Keegan, B. C.; Shearer, J.; Lehnert, N.; Shafaat, H. S. A Biochemical Nickel(I) State Supports Nucleophilic Alkyl Addition: A Roadmap for Methyl Reactivity in Acetyl Coenzyme A Synthase. *Inorg. Chem.* **2019**, *58*, 8969–8982.
(55) Romanini, D. W.; Francis, M. B. Attachment of Peptide Building Blocks to Proteins Through Tyrosine Bioconjugation. *Bioconjugate Chem.* **2008**, *19*, 153–157.
(56) Fourmond, V.; Hoke, K.; Heering, H. A.; Baffert, C.; Leroux, F.; Bertrand, P.; Léger, C. SOAS: A free program to analyze

electrochemical data and other one-dimensional signals. *Bioelectrochemistry* **2009**, *76*, 141–147.

(57) Laviron, E. General expression of the linear potential sweep voltammogram in the case of diffusionless electrochemical systems. *J. Electroanal. Chem. Int. Electrochem.* **1979**, *101*, 19–28.

(58) Jeuken, L. J. C.; McEvoy, J. P.; Armstrong, F. A. Insights into Gated Electron-Transfer Kinetics at the Electrode−Protein Interface: A Square Wave Voltammetry Study of the Blue Copper Protein Azurin. *J. Phys. Chem. B* **2002**, *106*, 2304–2313.

(59) Kozuch, S.; Martin, J. M. L. "Turning Over" Definitions in Catalytic Cycles. *ACS Catal.* **2012**, *2*, 2787–2794.

(60) Krishnan, S.; Armstrong, F. A. Order-of-magnitude enhancement of an enzymatic hydrogen-air fuel cell based on pyrenyl carbon nanostructures. *Chem. Sci.* **2012**, *3*, 1015–1023.

(61) Grabarek, Z.; Gergely, J. Zero-length crosslinking procedure with the use of active esters. *Analytical Biochemistry* **1990**, *185*, 131–135.

(62) Wang, L.; Sofer, Z.; Pumera, M. Will Any Crap We Put into Graphene Increase Its Electrocatalytic Effect? *ACS Nano* **2020**, *14*, 21–25.

(63) Léger, C.; Jones, A. K.; Albracht, S. P. J.; Armstrong, F. A. Effect of a Dispersion of Interfacial Electron Transfer Rates on Steady State Catalytic Electron Transport in [NiFe]-hydrogenase and Other Enzymes. *J. Phys. Chem. B* **2002**, *106*, 13058–13063.

(64) Warren, J. J.; Tronic, T. A.; Mayer, J. M. Thermochemistry of Proton-Coupled Electron Transfer Reagents and its Implications. *Chem. Rev.* **2010**, *110*, 6961–7001.

(65) Hexter, S. V.; Esterle, T. F.; Armstrong, F. A. A unified model for surface electrocatalysis based on observations with enzymes. *Phys. Chem. Chem. Phys.* **2014**, *16*, 11822–11833.

(66) Parkin, A.; Seravalli, J.; Vincent, K. A.; Ragsdale, S. W.; Armstrong, F. A. Rapid and Efficient Electrocatalytic CO2/CO Interconversions by Carboxydothermus hydrogenoformans CO Dehydrogenase I on an Electrode. *J. Am. Chem. Soc.* **2007**, *129*, 10328–10329.

(67) Mann, J. A.; Rodríguez-López, J.; Abruña, H. D.; Dichtel, W. R. Multivalent Binding Motifs for the Noncovalent Functionalization of Graphene. *J. Am. Chem. Soc.* **2011**, *133*, 17614–17617.

(68) Mondal, M. S.; Goodin, D. B.; Armstrong, F. A. Simultaneous voltammetric comparisons of reduction potentials, reactivities, and stabilities of the high-potential catalytic states of wild-type and distal-pocket mutant (W51F) yeast cytochrome c peroxidase. *J. Am. Chem. Soc.* **1998**, *120*, 6270–6276.

(69) Černocká, H.; Ostatná, V.; Paleček, E. Enzymatic activity and catalytic hydrogen evolution in reduced and oxidized urease at mercury surfaces. *Anal. Chim. Acta* **2013**, *789*, 41–46.

(70) Marracino, P.; Apollonio, F.; Liberti, M.; d'Inzeo, G.; Amadei, A. Effect of High Exogenous Electric Pulses on Protein Conformation: Myoglobin as a Case Study. *J. Phys. Chem. B* **2013**, *117*, 2273–2279.

SYNOPSIS TOC. A simple but effective covalent attachment method is developed for generating robust electrodes capable of prolonged aqueous hydrogen evolution using an artificial metalloenzyme catalyst.